GLOBAL AND LOCAL DEMAND LIMITS OF THIN REINFORCED CONCRETE STRUCTURAL WALL BUILDING SYSTEMS

C.A. Arteta[1], J. Sánchez[2], R. Daza[2], C. Blandon[3], R. Bonett[4], J. Carrillo[5], J. Velez[6]

[1] *Assistant professor, Universidad del Norte, Colombia carteta@uninorte.edu.co*

[2] *MSc Student, Universidad del Norte, Colombia*

[3] *Associate professor, Universidad EIA, Colombia*

[4] *Professor, Universidad de Medellin, Colombia*

[5] *Associate professor, Universidad Militar Nueva Granada, Colombia*

[6] *PhD Student, Universidad de Antioquia, Colombia*

Abstract

Industrialized construction system used in some Latin American countries are build based on elements which are of special interest because the geometry of their cross section, and layout of longitudinal reinforcement may facilitate the triggering of flexural-compression failures. This is so because of the excessive compressive demand on a thin-poorly-detailed web that arises due to seismic action. Given the large unsupported length of the web close to the critical section at the base, the extreme portions of these elements are also prone to lateral (out-of-plane) instability when subjected to cycling loading. This paper presents and analyzes a database of reinforced concrete thin-wall buildings representative of building archetypes in some countries in the southern hemisphere of the Americas. Variables of interest such as wall area index, fundamental period, flanged-wall cross section geometry, wall aspect ratio, reinforcing steel detailing, axial load ratio, building period, neutral axis depth, shear span ratio, among others, are analyzed in detail. A drift coupling factor is introduced to evaluate the impact of coupling of the surrounding system on individual walls. An archetype wall representative of the buildings in the database is selected by means of a multivariate statistical analysis. This prototype will serve as subject of laboratory testing. The paper also presents and discusses the results of a reversed-cyclic-loading experiments on a rectangular and T-shaped reinforced concrete thin-wall with aspect ratio of 3 and 3.7, respectively. The specimens are representative of the construction practice in intermediate seismic hazard areas in Colombia. Results suggest that this type of elements have limited ductility capacity, inferior to the expected behavior promoted by the building codes. Global and local deformation parameters from experimental data are discussed.

Keywords: building database; reinforced concrete; thin flanged wall; reversed-cyclic loading.

1. Introduction

Industrialized construction of multistory reinforced concrete (RC) wall buildings has become a common practice in Latin-American countries such a Colombia, Peru, Ecuador and Mexico. An important feature of this structural system is that architectural spaces are also bounded by the structural walls, which reduces the time of construction and the related cost. Therefore, structural engineers have pushed the usable limits of the structural walls by further reducing their thickness over the years. This trend has resulted in large unbraced length, increasing the slenderness ratio of the wall at the critical section. When portions of these thin wall sections are subjected to compressive strains, the risk of lateral instability arises [1]. Examples of unexpected damage of thin walls have been observed in column and wall tests [2-5] and in damaged structures during the 2010 Chile [6, 7] and 2011 New Zealand [8] earthquakes. This paper shows and discusses a thin-wall building database of Armenia, a city of Colombia, in Northern South America, located in a highly active seismic zone. The database comprises 65 flanged-walls of 28 multistory RC thin-wall building and is representative of building archetypes in the southern hemisphere of the Americas. Variables of interest are the wall area index, fundamental period, cross section geometry, wall aspect ratio, reinforcing steel detailing, axial load ratio, building period, neutral axis depth, shear span ratio, among others. The paper also presents and discusses the results of a reversed-cyclic-loading experiment on a rectangular reinforced concrete thin-wall with aspect ratio of 3 carried out in Colombia. Additional data is obtained from test carried out at EPFL and reported by Rosso et al [3]. Results suggest that this type of elements may have limited ductility capacity, inferior to the expected behavior promoted by the building codes

2. Thin wall building batabase

Armenia is a well-known seismic region in Colombia and is influenced by an active crustal faulting systems, as well as intermediate-to-deep subduction seismic hazard. Armenia was the closest (17 km) major city to the epicenter of the January 25th, 1999 "Eje Cafetero Earthquake". The Mw 6.2 event was located at 19 km of depth, with an estimated rupture area of 124 km^2 causing a significant number of death and damages [9]. The severity of these consequences motivated a rapid implementation of the latest building codes in Colombia at the time, NSR-98 [10], later superseded by NSR-10 [11] which is mainly adapted with minor changes from the ACI-318-08 [12]. Twenty-eight multistory thin-wall RC buildings blueprints were obtained for actual buildings in Armenia (Fig. 1). A database of this structures was built, focusing on the flange U-, L-, and T-shaped walls that sustain most of the seismic base shear. These elements are of special interest because the geometry of their cross section, and layout of longitudinal reinforcement may facilitate the triggering of flexural-compression failures. This is so because of the excessive compressive demand on a thin-poorly-detailed web that arises due to seismic action. Given the large unsupported length of the web close to the critical section at the base, the extreme portions of these elements are also prone to lateral (out-of-plane) instability when subjected to cycling loading.

Fig. 1 –Pictures of thin-wall buildings in the database.

2.1 Global geometry parameters

Table 1 shows attributes of buildings in the database. Global geometric variables are: H_w = the building height, B_t = the plan transverse (shorter) direction, and B_l = the plan longitudinal (longer) direction. Dimensions B_t and B_l correspond to the sides of a rectangle were the building can be inscribed. Variable R corresponds to the response modification factor that accounts for the expected inelastic behavior during design and the over-strength of the structure. Fig. 2 shows histograms of the number of stories and building aspect ratios H_w/B_t and H_w/B_l. The typical aspect ratio in the shorter direction of the building (e.g. H_w/B_t) is approximately 2, which is close to the aspect ratio for damaged wall buildings after the Chile 2010 earthquake [13]. The distribution of the number of stories shows that approximately 30% of the buildings are shorter than 5 stories, and that approximately 45% of them have between 10 and 15 stories. It is worth noting that the typical story height is 2.4 m.

Table 1 – Global geometry parameters of the buildings in the Armenia database

ID	# Story	Year	H_w [m]	R	NEHRP Soil Profile	B_x [m]	B_y [m]	$B_t = B_{min}$ [m]	H_w/B_t	H_w/B_l
1	12	2015	30.0	-	-	25.9	17.7	17.7	1.7	1.2
2	15	2015	40.3	5	D	35.6	15.5	15.5	2.6	1.1
3	14	2015	33.1	-	D	13.4	35.4	13.4	2.5	0.9
4	12	2015	31.4	4	E	30.5	12.8	12.8	2.5	1.0
5	5	2015	12.5	5	D	16.7	14.3	14.3	0.9	0.7
6	14	2015	38.4	5	D	38.0	20.3	20.3	1.9	1.0
7	18	2015	43.2	5	D	14.2	35.1	14.2	3.0	1.2
8	15	2013	37.7	5	D	29.9	7.7	7.7	4.9	1.3
9	15	2015	38.8	5	E	34.8	11.6	11.6	3.4	1.1
10	16	2013	38.9	-	D	16.2	43.6	16.2	2.4	0.9
11	4	2014	10.0	3.2	D	17.6	6.0	6.0	1.7	0.6
12	5	2013	12.5	4	D	21.9	10.3	10.3	1.2	0.6
13	5	2013	12.5	5	D	17.4	13.0	13.0	1.0	0.7

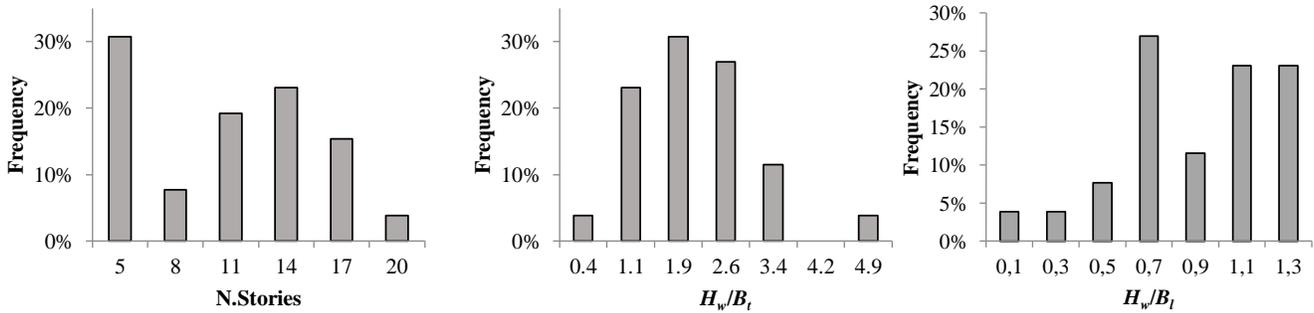| ID	# Story	Year	H_w [m]	R	NEHRP Soil Profile	B_x [m]	B_y [m]	$B_t = B_{min}$ [m]	H_w/B_t	H_w/B_l
14	8	2014	20.0	4	D	43.3	17.5	17.5	1.1	0.5
15	5	2011	12.5	-	-	23.5	15.3	15.3	0.8	0.5
17	3	2011	7.5	5	D	60.6	20.8	20.8	0.4	0.1
18	14	2012	30.7	2.64	D	32.4	11.4	11.4	2.7	0.9
19	9	2012	22.4	4	D	41.3	18.4	18.4	1.2	0.5
20	13	2012	37.5	-	D	30.3	17.6	17.6	2.1	1.2
21	11	2012	24.7	-	D	45.1	17.0	17.0	1.5	0.5
22	10	2012	27.7	-	-	29.8	13.6	13.6	2.0	0.9
23	5	2013	12.5	5	D	18.8	13.1	13.1	1.0	0.7
24	9	2013	22.4	4	D	33.8	14.3	14.3	1.6	0.7
25	7	2013	17.5	5	D	23.7	36.7	23.7	0.7	0.5
26	5	2013	12.5	4	E	53.7	17.6	17.6	0.7	0.2
27	10	2014	31.6	5	D	40.1	21.7	21.7	1.5	0.8
28	9	2015	22.5	5	D	49.2	12.7	12.7	1.8	0.5

Fig. 2 – Global geometric variables: number of stories and building aspect ratio.

One variable that has been correlated in the past with damage during earthquake events is the local wall area index (LWAI) of a building. For a given direction, the LWAI of a building is defined as the total area of wall webs supporting the shear demand in that direction, divided by the total area of the first floor. The global wall area index (GWAI) is defined as LWAI/(Number stories). This index is the ratio between the first story wall area and the total area being supported by it (i.e. above it). According to the scattergram in Fig. 3, the indices in either direction are similar. The LWAI typically ranges between 1.5% and 6% with an average value of 3.6%, while the GWAI ranges between 0.15% and 1.3% with an average value of 0.5%. Sozen [14] studied the dynamic characteristic a small-scale RC wall model subjected to seismic shaking, and contrasted the results with the building characteristics in a data base constructed by [15] after the 1985 Viña del Mar earthquake in Chile. According to this study, a plausible explanation for the good behavior of the wall-buildings observed after the 7.8 magnitude event was them having a LWAI larger than 3%. Jünemann et al. [13] report mean wall area index (averaged over all stories) of 2.8% and 2.9% for the longitudinal and transverse direction of the damaged wall buildings after the 2010 Chile earthquake.
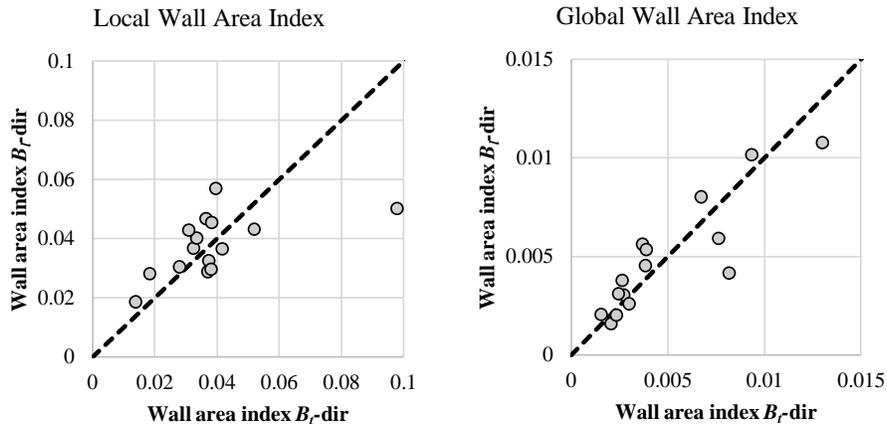

Fig. 3 – LWAI and GWAI in the two principal direction.

2.2 Selection of flanged-walls of interest

Selection of the flanged-wall of interest was based on the analysis of 17 three-dimensional elastic models of the buildings in Table 1. These models were constructed in the computer program ETABS® [16]. The structures were modeled with nominal material characteristics and the geometry found in the geometric and reinforcement layouts. Walls were modeled with thin-shell elements to account for the complete stiffness of U-, L-, and T-shaped wall segments. With this strategy, the modeling of a flanged wall loaded along its web axis is able to account for the out-of-plane bending action of the flange. Cracking was modeled by modifying the membrane stiffness coefficients of the sections. The buildings were analyzed under code-based equivalent lateral loading in two orthogonal directions to simulate uncoupled seismic action. The purpose of this analysis was to obtain the relative contribution provided by each wall segment to the base shear of the building in each direction. For each building, the walls contribution to the total base shear were organized in descending order. A first set of walls of interest comprised those in the upper portion of the list contributing to 50% of the total base shear in each direction. From this subset, only the flanged walls with large contribution in the direction compressing the web were selected (Fig. 4). A total of 65 individual flanged-walls of interest are analyzed in this paper.
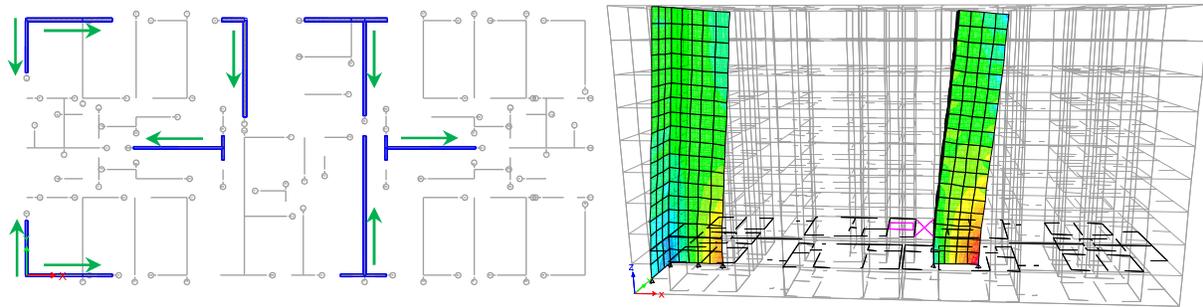

Fig. 4 – Isolation of flange-walls of interest in several direction for building 22 (left); vertical stress field on two flanged walls under lateral loading compressing the web (building 28).

2.3 Fundamental period of the buildings

Dynamic modal analyses were also performed to determine the fundamental period in the two main directions of the buildings. Fig. 5 shows plots of fundamental period versus geometric variable $\sqrt{(H_w^3/B_i)}$, where B_i is the length of the building parallel to the direction of analysis. The plots show a good correlation for individual direction analysis. For the longitudinal direction (i.e. parallel to B_l), the period of the building is adequately approximated by $T_l = 0.02\sqrt{\dfrac{H_w^3}{B_l}}$, while for the short (transverse) direction it can be approximated by $T_t = 0.01\sqrt{\dfrac{H_w^3}{B_i}}$.
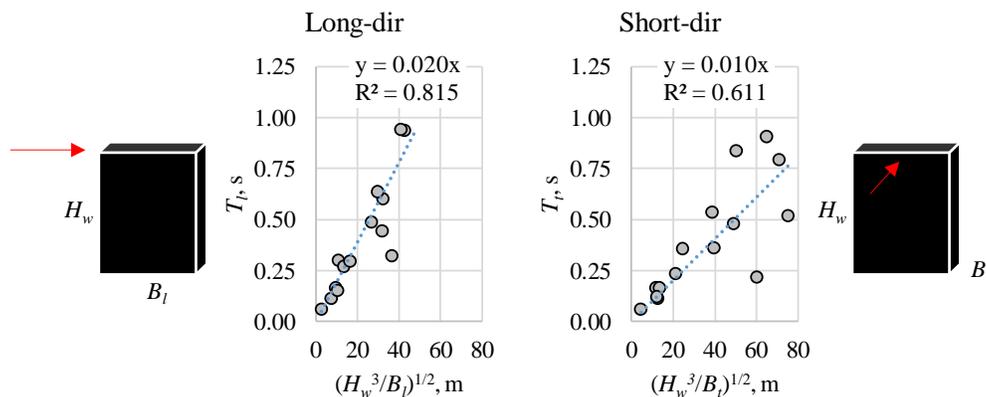

Fig. 5 – Fundamental period versus global geometric variables.

2.4 Cross section geometry and reinforcement layout

For an individual flanged wall, its aspect ratio (AR) is defined as the ratio of the wall height (H_w) and its length (l_w). Variable l_w varies between 2 m and 8 m, and the typical aspect ratio is close to 5. The wall thickness (t_w) variable takes six discrete values in the database: 80, 100, 120, 150, 180, and 200 mm, with an apparent concentration at 120 and 150 mm (Fig. 6a). Fig. 6b summarizes the relative frequency of steel layers in the web. The data is organized by wall thickness. Approximately 40% of all walls have 2 layers of welded wire mesh in the web. For walls with $t_w \geq 150$mm, this number increases to 65%, approximately.
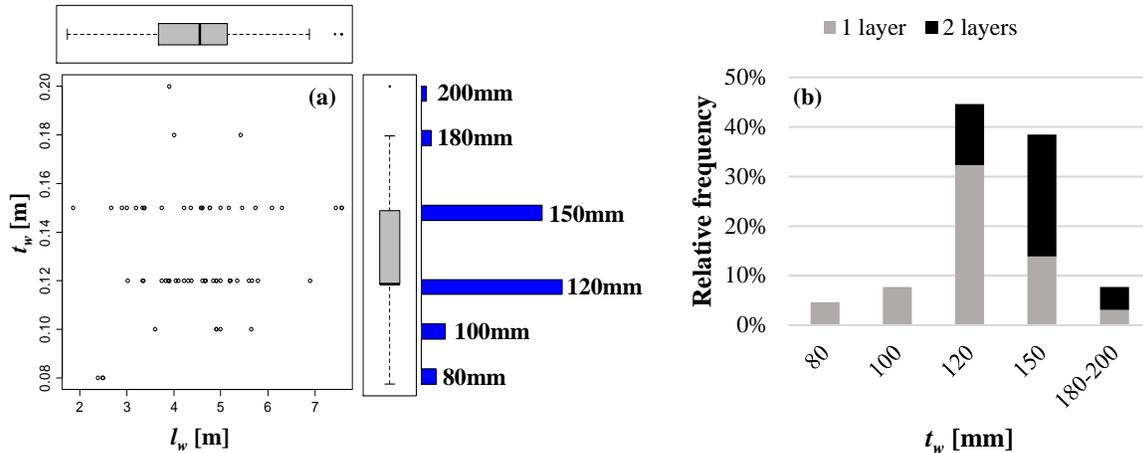

Fig. 6 – Web thickness and reinforcing layers: (a) thickness versus length of the wall; (b) number of web steel layers per wall thickness.

All specimens have distributed steel in the web and the flange. Excluding outliers, longitudinal steel ratio of distributed steel in the web (ρ_w) varies between $0.2\% \leq \rho_w \leq 0.7\%$, with typical value of 0.25% (minimum code requirement). All flanged walls are classified into six categories according to the layout of reinforcement in their cross section. Fig. 7 depict a representative scheme of each type. Type A cross sections only have distributed steel in the web and the flange, with not special transverse reinforcement detailing in the boundaries. Type B and C comprise specimens with additional longitudinal steel ($A_{s,BE}$) in the boundary region of the web, with not special transverse reinforcement detailing there. These may or may not have special transverse reinforcement detailing and/or additional longitudinal steel in the flange side. Type D and F specimens have additional longitudinal steel in the boundary region of the web and also include special transverse reinforcement detailing there. These may or may not have special transverse reinforcement detailing and/or additional longitudinal steel in the flange side. Type E specimens have special transverse reinforcement detailing in the boundary region with no additional longitudinal steel there. These may or may not have special transverse reinforcement detailing and/or additional longitudinal steel in the flange side. The average thickness of the walls with special transverse reinforcement detailing in the boundary of the web (e.g. Type D, E and F) is 0.14 m, with a typical value (mode) of 0.12 m. The relative frequency of every type of cross section is: A 34%, B and C 28%, D and F 28% and E 10%. The flange longitudinal reinforcement, $A_{s,f}$, is a variable of interest because it affects the neutral axis depth when a flanged-wall is loaded in the direction compressing the stem (i.e. generating flexural-tensile demand on the flange). The relative distribution of area of steel in the flange follows a Gamma distribution with mean equal to 21 cm^2.

2.5 Axial loading

The axial load of each wall was estimated using the mathematical models in ETABS. The dead load (D) of the models included the self-weight of the elements (e.g. walls, slabs, and beams) and an additional superimposed load of 1.6 kN/m^2 which accounts for other architectural and mechanical permanent weights. The live load (L) was 1.8kN/m^2 as defined for residential buildings in NSR-10. The load combination used for the estimation of the axial load is 1D+0.25L. The axial load ratio (ALR) of each wall is defined as $ALR=P/A_g f'_c$, where A_g is the gross cross section area of the wall, and f'_c is the nominal concrete strength. Fig. 8 shows the relative frequency of variable ALR. The distribution has a negative skew with mode of 7% approximately. It is also shown in the figure

that the ALR is positively correlated with wall height, and can be approximated as $ALR \approx H_w/500$, where H_w is in meters).

2.6 Approximation of the neutral axis depth

Fig. 9 shows a simple model of the equilibrium of internal and external forces associated to axial load and moment demand on a flanged-wall cross section which results in a neutral axis depth defined by Eq. 1.

$$c = \frac{T_{s,f} + T_{s,w} + P - C_s}{\alpha_1 \beta_1 f'_c t_w} \tag{1}$$

where $T_{s,f}$ is the tensile force in the flange, C_s is the compressive force in the boundary steel of the web, and variables α_1, and β_1 are rectangular stress block parameters. Fig. 9 also shows the distribution of the neutral axis depth normalized by the wall length (c/l_w). The modes of the fitted probability density functions are in the range of $0.20 \leq c/l_w \leq 0.25$. Deep neutral axes are associated to large flexural compressive strains, and may also enable out-of-plane instability in a longer portion of the web. The scattergram in Fig. 9 shows a highly correlated relationship between c/l_w and ALR.
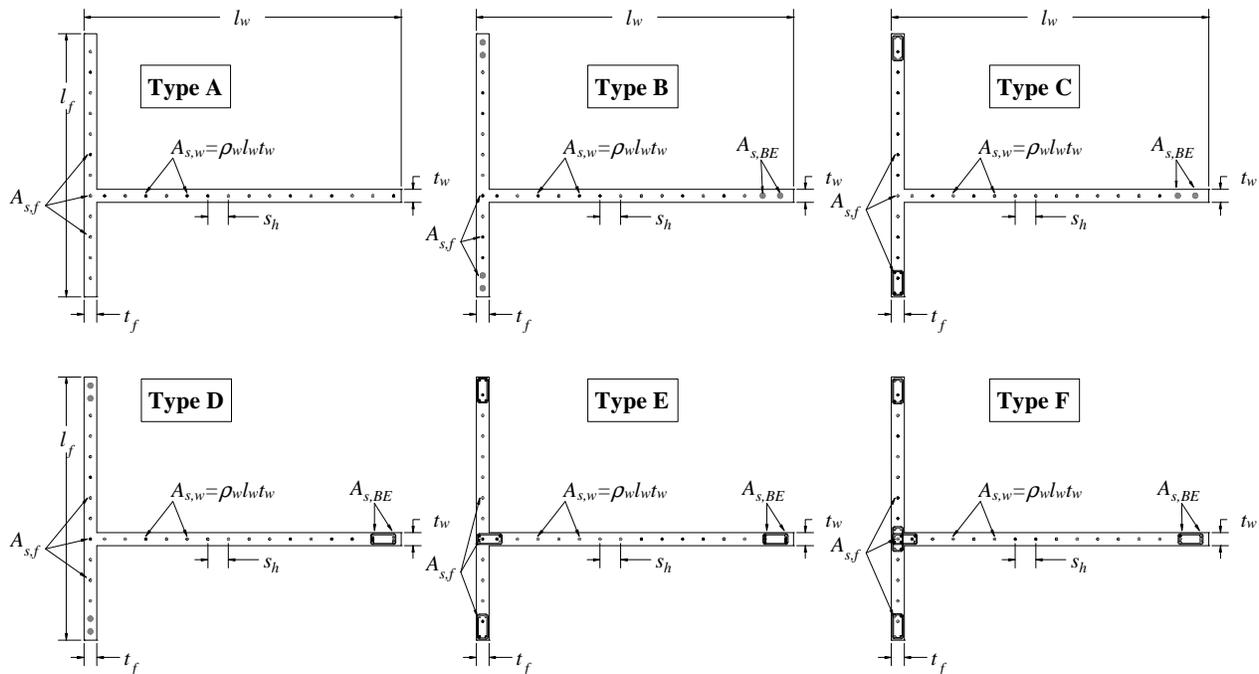

Fig. 7 –Types of reinforcement layout

2.7 Drift coupling, shear span (M/V) and shear span ratio (M/Vl_w)

Drift coupling of walls undergoing lateral displacement is a phenomena of interest because it impacts the displacement demand, as well as the shear and moment distribution along the height of the walls. When the whole structure sways in one direction, coupling in a single wall element is evidenced by the double curvature form of its displaced shape (in contrast with the single curvature displacement of a cantilever). In the moment diagram distribution, coupling is evidenced by the appearance of an inflection point upstairs. Fig. 10 depicts a cantilever wall model under lateral seismic demand. The purpose of this model is to relate global demand parameters such as base shear (V_b) and base moment (M_b) to geometric variables such as wall aspect ratio, AR. The shear span is defined as the ratio M/V, while the shear span ratio is a non-dimensional quantity of the form M/Vl_w. This expression represents, to some extent, the relative contribution of shear and flexural demand on the wall. It is worth noting that the intensity of the acting lateral loads in Fig. 10 is adjusted in such a manner that the base shear in the model is V_b. Demand on the cantilever wall comprises and inverted triangular lateral loading, but an reversed concentrated load at the roof is added with the aim of representing coupling with an adjacent system (e.g. frames, or other walls) [17]. The reversed concentrated load is a portion of the base shear with magnitude ηV_b, where η is

defined in this database as the *coupling factor*. Under this load pattern, the moment distribution along the length of the wall is quadratic with an inflection point at height h_{M0}, which arises from the double curvature displacement of the wall due to the pull action upstairs. The corresponding shear reversal occurs at height h_{V0}. Resulting shear span, and shear span ratios are $(M/V)=(2-\eta)/3H_w$ and $(M/Vl_w)=(2-\eta)/3AR$.
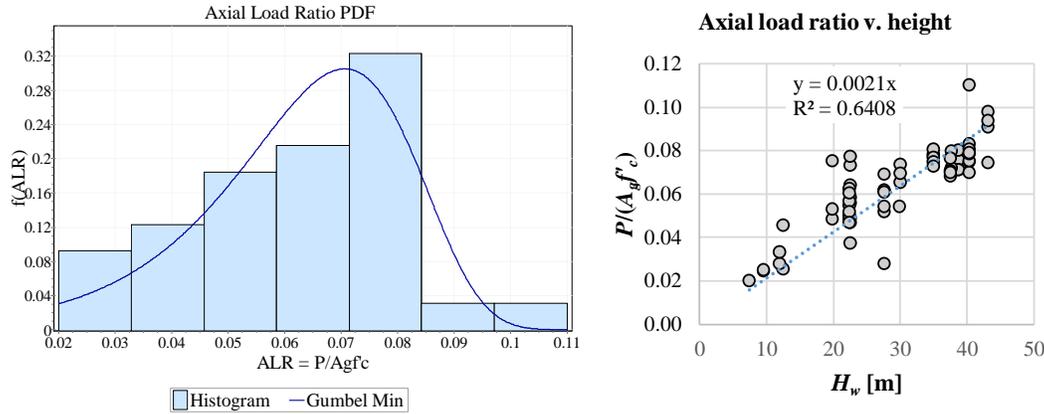

Fig. 8 – Axial load ratio distribution (ALR, left), and ALR correlation with building height.
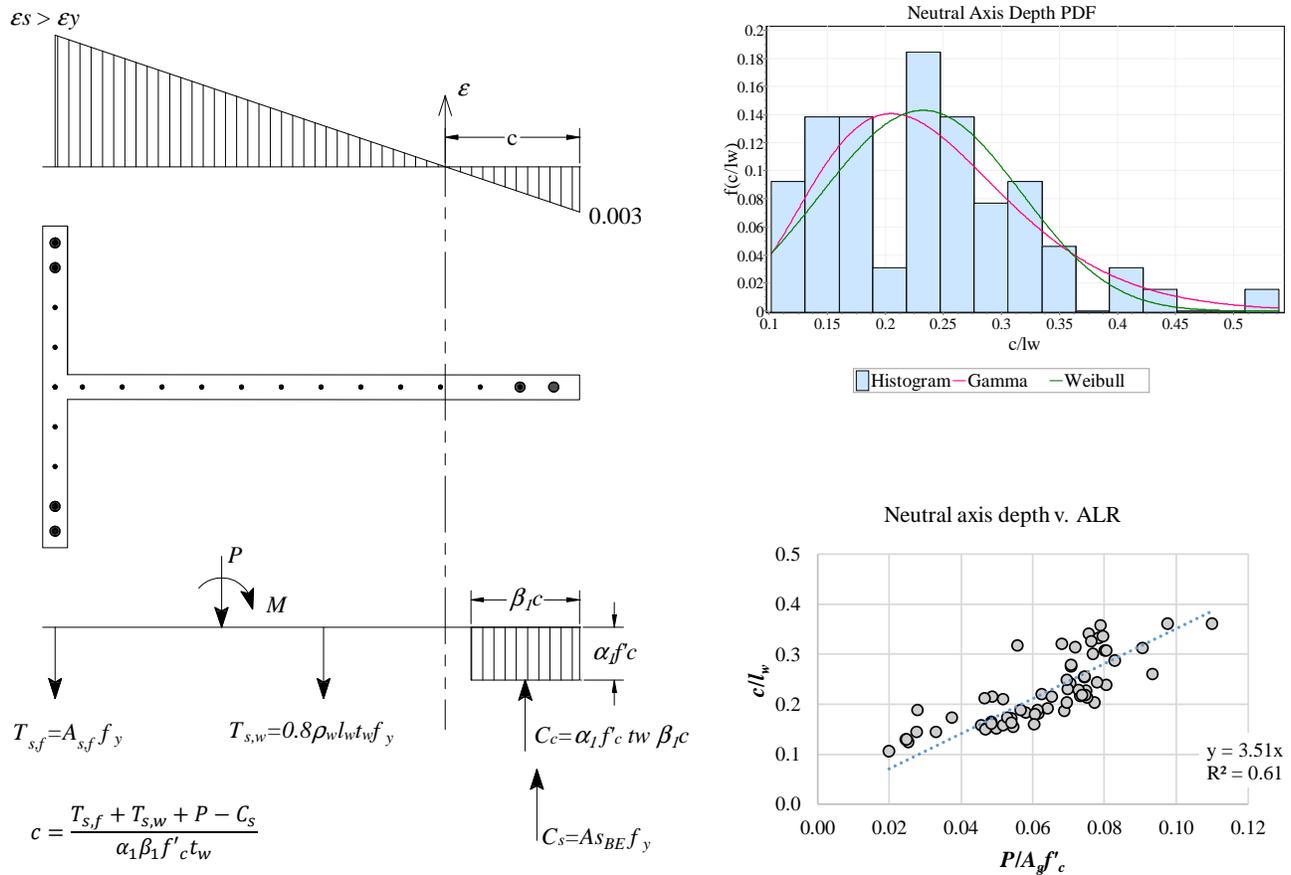

Fig. 9 – Compatibility and equilibrium in the cross section of flanged-walls under axial load and moment compressing the web end (left); normalized neutral axis depth distribution (top right); normalized neutral axis depth versus ALR (bottom right).

Model C

$$\frac{M}{V} = \frac{(2-\eta)}{3} H_w$$

$$\frac{M}{V l_w} = \frac{(2-\eta)}{3} \frac{H_w}{l_w} = \frac{(2-\eta)}{3} AR$$

$$\frac{M}{V H_w} = \frac{(2-\eta)}{3}$$

$$V(h) = 0 \ @ \ \frac{h_{V0}}{H_w} = \frac{1}{\sqrt{1+\eta}}$$

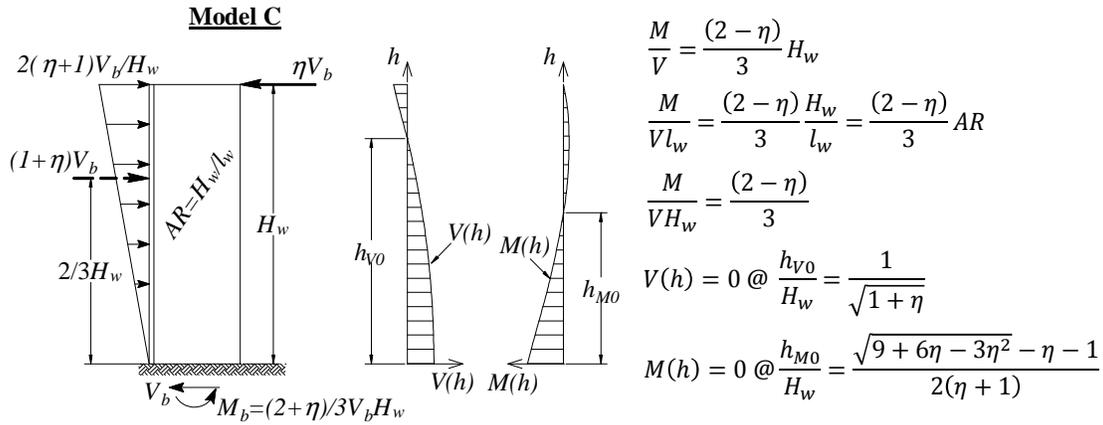$$M(h) = 0 \ @ \ \frac{h_{M0}}{H_w} = \frac{\sqrt{9+6\eta-3\eta^2}-\eta-1}{2(\eta+1)}$$

Fig. 10 – Response parameters of cantilever wall models under seismic loading.

From the linear elastic analyses, the base shear and the moment at the base of each wall was recorded. This was done for the direction compressing the edge of the web of each flanged-wall in the database. Fig. 11 show values of static shear span ratios, M/Vl_w, for the flanged-wall of the database. The typical shear span ratio is close to 2, which is a result of the coupling among the individual walls in a building. To further study coupling of the walls, factor η is estimated from the aforementioned values of shear span ratio, using the formulations in Fig. 10. Given M/Vl_w, and the aspect ratio of the wall, $\eta = 2 - \frac{2}{AR}\frac{M}{Vl_w}$. Coupling factor η is plotted with corresponding values of l_w in Fig. 11Fig. 10. It is observed that coupling reduces as the wall length increases, which is interpreted that stiffer walls are less affected by the surrounding system.
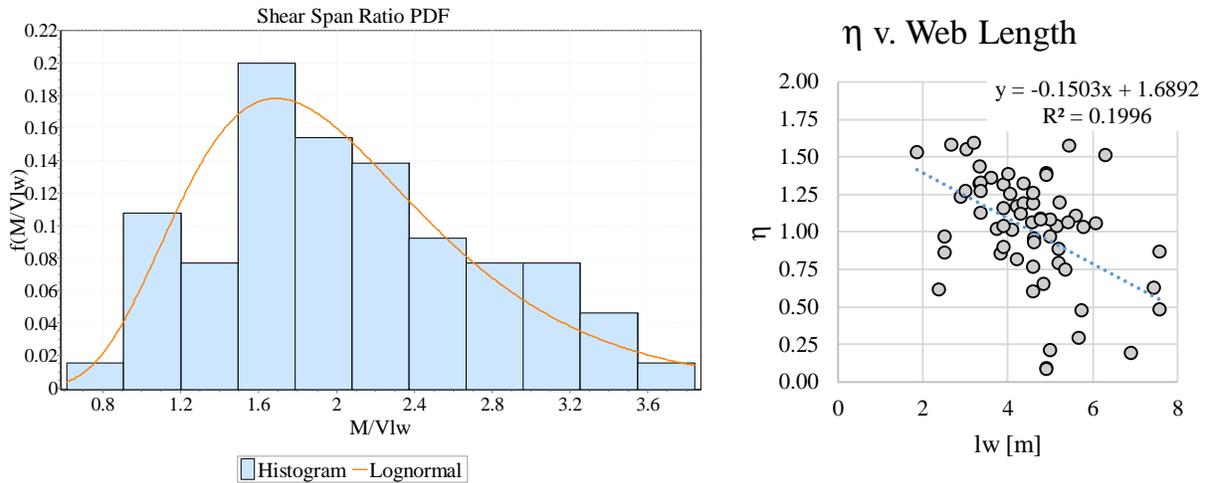

Fig. 11 – Shear span ratio distribution (left); coupling factor, η, versus web length relationship (right).

2.8 Prototype wall

An archetype wall for the city of Armenia was defined based on the following variables: (1) l_w = wall length; (2) ALR = axial load ratio; (3) $A_{s,f}$ = area of steel in the flange; and (4) M/Vl_w = shear span ratio. For this, the 65 walls of interest were binned and the number of realizations of various combinations of the variables above was counted. This ensured that the selected wall was representative of the wall in the database and not a mere independent selection of variables. A simple statistical multivariate analysis allowed describing the selection space in Fig. 12. Analysis of this data showed that the variables of selection are in the range 3.0 m $\leq l_w \leq$ 5.3 m, 3.8% $\leq$ ALR $\leq$ 9.2%, 1.7 cm2 $\leq A_{s,f} \leq$ 15.8 cm^2, 0.6 $\leq M/Vl_w \leq$ 2.6, including the extreme values of the bins they belong to. An

archetype wall representative of the thin-wall building database has the following parameters: $l_w = 3.5$ m, ALR = 8%, $A_{s,f} = 7.74$ cm^2, $M/Vl_w = 2$, $M/V = 7$. Three models of this wall are due experimental testing by the end of 2016.
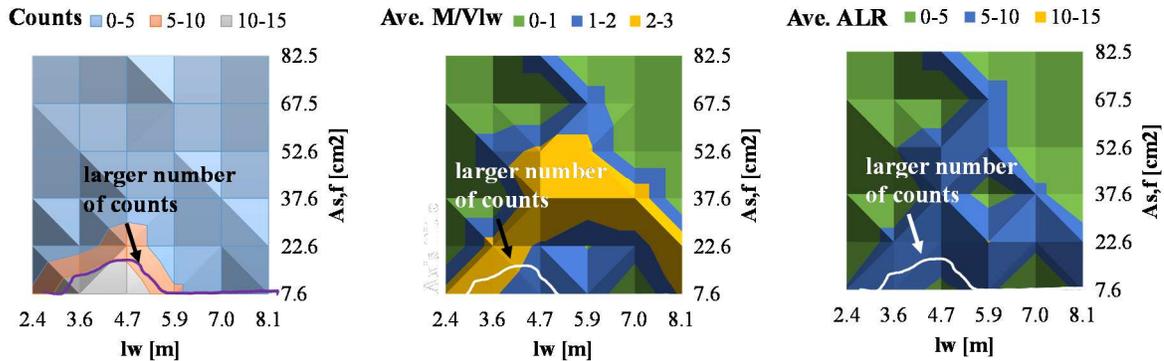

Fig. 12 – Selection space of the wall prototype.

3. Reinforced concrete thin wall experimental response

3.1 Test unit

The test specimen presented in the following section was selected to characterize the most critical wall in terms of slenderness and reinforcement details identified during the analyses of a thin-wall building database of the city of Medellín, Colombia (located in an intermediate seismic hazard zone). The specimen characterizes a rectangular wall of a seven-story building (18 m in height) with an increased interstory height to evaluate a critical case for out of plane instability. The dimensions of the specimen $1200 \times 3600 \times 80$ mm (length, height, thickness) corresponding to AR = 3 and M/Vl_w ratio of 3.1. The axial force applied was approximately 16% of the compressive strength of the gross section ($0.16 f'_c A_g$). The nominal compressive strength of concrete was 21 MPa. Fig. 13 shows the cross section and reinforcement layout of the specimen. According to the database, this kind of walls do not have boundary elements and the main web reinforcement correspond to a welded wire mesh (wires having 5.5 mm of diameter with spacing of 150 mm, which is equivalent to reinforcement ratio of 0.19%). At the ends of the wall, two # 5 bars (5/8 in. of diameter) were included.

3.2 Test setup

The wall specimen was tested under quasi-static cyclic loading. The test was carried out using a reaction frame and strong floor at the Laboratory of the "Universidad EIA" (Colombia). At the wall head, one servo-controlled hydraulic actuator was installed for applying the horizontal displacement history. Steel beams and rollers placed 3.4 m above the foundation guided the horizontal displacement and restrained out-of-plane displacements due to accidental eccentricity. The axial load was applied through unbonded post-tensioning strands located on either side of the wall and distributed over its entire length. During the testing, the behavior of the wall was monitored with strain gauges to measure strain deformations, linear variable differential transformers (LVDT) to record in-plane and out-plane displacements and rotations, and load cells to measure lateral and axial load.
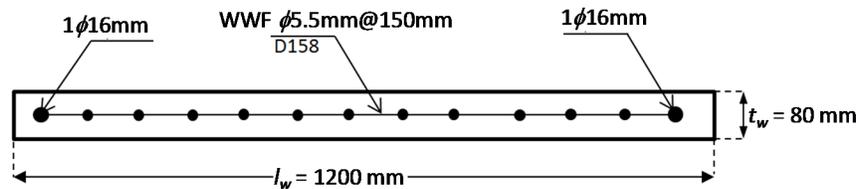

Fig. 13 – Detail of the wall specimen.

The first step of the testing protocol was the application of the axial load (320 kN), which was kept approximately constant throughout the testing. A slight variation of the total exerted axial was observed due to shortening and lengthening of the tendons. Subsequently, four force-controlled cycles were applied: two cycles

for 50% and two for 75% of the computed nominal yield force, respectively. The next cycles were displacement-controlled, with target displacement ductility equal to +1 and -1 (μ_Δ= 1.0), corresponding to a top lateral displacement of 15 mm. The ductility factor kept increasing until the wall failed (μ_Δ = 1.5, 2.0, 3.0).

3.3 Experimental results

Force-displacement hysteresis curves and the force–displacement envelopes are shown in Fig. 14. The nominal yield displacement was determined as 4/3 of the average peak displacement reached during the first cycle which corresponds to 75% of the yielding force [18]. The yielding displacement was close to 18 mm in both directions (~0.45% of drift) and the corresponding force was 67 kN (93.3% of maximum load capacity) and 60 kN (81.7% of maximum load capacity) for each direction of loading. The load and displacement capacity at peak load were 71.8 kN and 25 mm (~0.62% of drift) and 73.4 kN and 30 mm (~0.65% of drift) for each direction of loading. Ultimate displacement was 49 mm (~1.1% of drift) and the corresponding displacement ductility factor was close to 2.5. This value of drift capacity is close to the design limit of 1% proposed by NSR-10 indicating a limited displacement capacity and significant level of damage for limited displacement demands. Failure was preceded by a significant out of plane deformation and it was characterized by spalling of concrete at the lower compressed wall edge followed by a rapid out of plane shear failure induced by the out of plane deformation (Fig. 15).
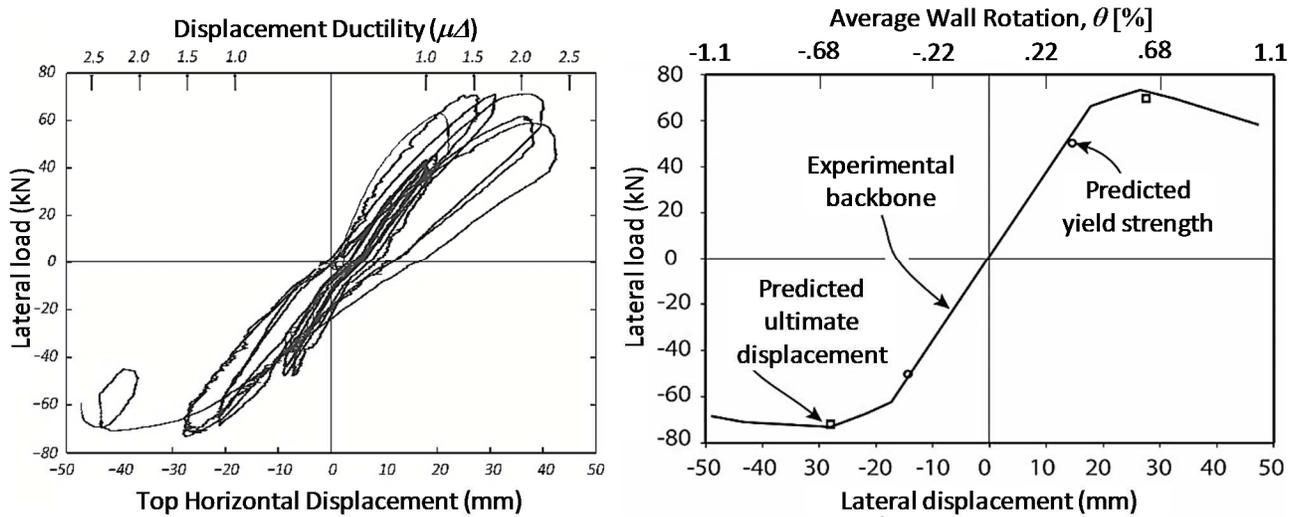

Fig. 14 – Hysteresis curve and corresponding envelope of response.

Fig. 15 – Final state of the wall.

4. Discussion

Tests at the EPFL reported by Rosso et al. [3], were based on the same building database for the city of Medellín, and comprised a T-shaped section with a 2.7 m x 0.08 m web and a 0.08m x 0.35 m flange. ALR was 5% and M/Vl_w ratio of 3.7. The steel distribution was similar to the test discussed in the previous section, with only one layer and #5 rebar concentrated at both ends. This wall was tested to evaluate the behavior of the longest walls within a building that control the seismic behavior. Significant out-of-plane displacement was also observed for this wall and failure occurred for a lateral drift of 0.7% while the thin web was in compression. Both tests indicate that under certain conditions, out-of-plane instability seem to induce a significant reduction of the deformation capacity of the walls.

Average strains obtained from LVDT placed along the failure section for the wall TW1 tested at EPFL show significant compression strains close to 0.008 and tensile strains close to 0.038 (Fig. 16). These values could be used to calibrate numerical model and define performance limits for these type of walls. There is however a need to obtain additional experimental data considering different reinforcement, geometry and loading conditions to have a better level of confidence on the behavior of thin walls. Specimens defined based on the statistical procedure previously described will be tested to complement data currently available.
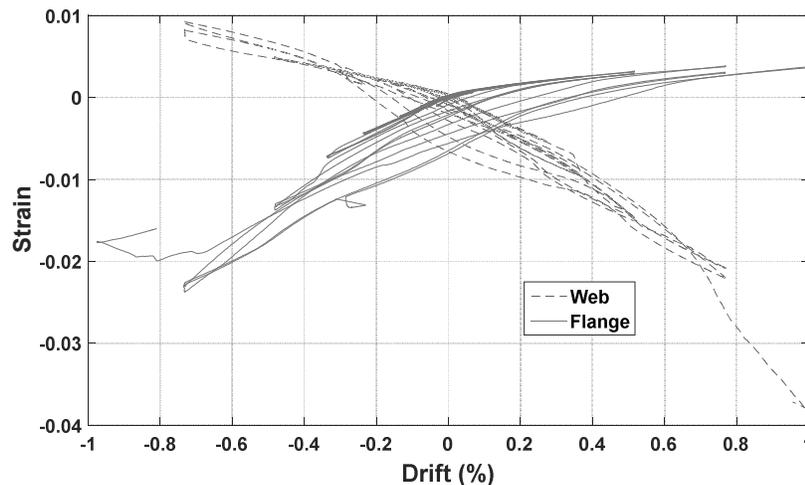

Fig. 16 –EPFL wall average strain.

5. References

1.   Parra, P. and J. Moehle. *Lateral buckling in reinforced concrete walls*. in *Tenth US Natl Conf Earthq Eng, Anchorage, Alaska*. 2014.

2.   Chai, Y.H. and D.T. Elayer, *Lateral stability of reinforced concrete columns under axial reversed cyclic tension and compression.* ACI Structural Journal, 1999. **96**(5): p. 780-789.

3.   Rosso, A., J.P. Almeida, and K. Beyer, *Stability of thin reinforced concrete walls under cyclic loads: state-of-the-art and new experimental findings.* Bulletin of Earthquake Engineering, 2016. **14**(2): p. 455-484.

4.   Welt, T.S., *Detailing for compression in reinforced concrete wall boundary elements: experiments, simulations, and design recommendations*. 2015, University of Illinois at Urbana-Champaign.

5.   Acevedo, C., et al. *Seismic Vulnerability of Non-special Boundary Element of Shear Wall under Axial Force Reversals*. 2010. 16.

6.   Wallace, J.W., et al., *Damage and Implications for Seismic Design of RC Structural Wall Buildings.* Earthquake Spectra, 2012. **28**(S1): p. S281-S299.

7.   Alarcon, C., et al., *Characteristics and displacement capacity of reinforced concrete walls in damaged buildings during 2010 Chile earthquake.* Bulletin of Earthquake Engineering, 2015. **13**(4): p. 1119-1139.

8.   Sritharan, S., et al., *Understanding Poor Seismic Performance of Concrete Walls and Design Implications.* Earthquake Spectra, 2014. **30**(1): p. 307-334.

9.   Cardona, O., et al., *Estudio sobre desastres ocurridos en Colombia: Estimación de pérdidas y cuantificación de costos.* Evaluación de Riesgos Naturales (ERN), Bogotá[Links], 2004.

10.   Comité-AIS-100, *Normas Colombianas de Diseño y Construcción Sismo Resistente, NSR-98.* 1998, Asociación Colombiana de Ingeniería Sísmica.

11.   Comité-AIS-100, *Reglamento Colombiano de Construcción Sismo Resistente, NSR-10.* 2010, Asociación Colombiana de Ingeniería Sísmica.

12.   ACI-Committee-318, *Building Code Requirements for Structural Concrete and Commentary (ACI 318-08).* 2008, American Concrete Institute: Farmington Hills, MI. p. 473.

13.   Junemann, R., et al., *A statistical analysis of reinforced concrete wall buildings damaged during the 2010, Chile earthquake.* Engineering Structures, 2015. **82**: p. 168-185.

14.   Sozen, M.A. *Earthquake response of buildings with robust walls.* in *Fifth Chilean Conference on Seismology and Earthquake Engineering.* 1989. Santiago de Chile.

15.   Ridell, R., S.L. Wood, and J.C. de la Llera, *The 1985 Chile earthquake: structural characteristics and damage statistics for the building inventory in Viña del Mar.* 1987, University of Illinois Engineering Experiment Station. College of Engineering. University of Illinois at Urbana-Champaign.

16.   CSI, *ETABS Nonlinear. Extended ThreeDimensional Analysis of Building Systems.* 2011, Computers and Structures Inc.: Berkeley, CA.

17.   Priestley, M.J.N., G.M. Calvi, and M.J. Kowalsky, *Displacement Based Seismic Design of Structures.* 2007, Pavia: IUSS Press.

18.   Priestley, M. and R. Park, *Strength and ductility of concrete bridge columns under seismic loading.* ACI Structural Journal, 1987. **84**(1).